Influence of the asymmetry parameter and dissipation coefficient of the K coordinate on different aspects of fission of excited compound nuclei

H. Eslamizadeh* and N. Abdollahi

Department of Physics, Faculty of Basic Sciences, Persian Gulf University, P.O. Box 7516913817, Bushehr, Iran

(Received 13 November 2017; revised manuscript received 1 January 2018; published 20 February 2018)

The dynamics of fission of the excited compound nuclei ^{256}Fm, ^{215}Fr, ^{187}Ir, ^{172}Yb, ^{162}Yb, and ^{142}Ce produced in fusion reactions with 158.8 MeV ^{18}O has been studied by solving three- and four-dimensional Langevin equations with dissipation generated through the chaos weighted wall and window friction formula. The constant dissipation coefficients of K, $\gamma_K = 0.077$ (MeV zs)$^{-1/2}$, $\gamma_K = 0.2$ (MeV zs)$^{-1/2}$ and a nonconstant dissipation coefficient of K have been used to reproduce the experimental data for both symmetric and asymmetric splitting of the fissioning systems. The average kinetic energies of fission fragments, the pre-scission neutron multiplicities, the fission time, and the variances of the mass and kinetic energy of fission fragments are calculated for the excited compound nuclei ^{256}Fm, ^{215}Fr, ^{187}Ir, ^{172}Yb, ^{162}Yb, ^{142}Ce, and results of the calculations are compared with each other and with the experimental data. Comparison of the theoretical results with the experimental data calculated by using different values of γ_K shows that the difference is small between the results of calculations for symmetric and asymmetric simulations of the fission process of excited intermediate nuclei, whereas for heavy compound nuclei the difference is slightly high. In other words, the effect of the asymmetry parameter on the fission process of intermediate nuclei is smaller than the effect on heavy nuclei. Furthermore, we show that the pre-scission neutron multiplicity decreases rapidly with increasing fragment asymmetry.

DOI: 10.1103/PhysRevC.97.024614

I. INTRODUCTION

The characteristics of fission of excited nuclei produced in heavy-ion fusion reactions have been studied extensively both theoretically and experimentally over the years. Statistical and dynamical descriptions of the fission process are often used to explain different fission characteristics (see, for example, Refs. [1–20]). Many researchers searching to describe the different features of the fission process of excited compound nuclei assumed that compound nuclei have zero spin about the symmetry axis, whereas this assumption is not consistent with statistical models and with dynamical treatment of the orientation degree of freedom, as pointed out by Lestone [21]. The authors of Ref. [22] also stress that a large volume of heavy-ion-induced-fission data needs to be reanalyzed by applying a dynamical treatment of the orientation degree of freedom. The dynamical models based on the multidimensional Langevin equations have been extensively and rather successfully used to solve many problems of collective nuclear dynamics in heavy-ion fusion-fission reactions. Recently, four-dimensional (4D) Langevin equations with a constant dissipation coefficient for the orientation degree of freedom (the K coordinate) have been used to calculate different aspects of fusion-fission reactions [23–25]. In our previous paper [20], we also used the 4D dynamical model based on the Langevin equations to calculate the evaporation residue cross section, the anisotropy the angular distribution of fission fragments, the fission probability, the mass-energy distribution of fission fragments, and the average pre-scission neutron multiplicity for the compound nucleus ^{210}Rn in a wide range of excitation energy. In our calculations [20], we considered the dissipation coefficient of K as a free parameter and its magnitude is inferred by fitting measured data on the evaporation residue cross section and the anisotropy of the angular distribution of fission fragments.

In the present investigation, we use the four-dimensional (4D) and three-dimensional (3D) dynamical models based on Langevin equations to calculate a number of other fission features of the excited nuclei in a wide range of mass number. In our calculations, we use the constant and non-constant dissipation coefficients of K to reproduce the experimental data in the fission process of the excited compound nuclei ^{256}Fm, ^{215}Fr, ^{187}Ir, ^{172}Yb, ^{162}Yb, and ^{142}Ce produced in fusion reactions with 158.8 MeV ^{18}O. In the 4D dynamical model, we use three collective-shape coordinates (c,h,α) plus the projection of total spin of the compound nucleus on the symmetry axis K and in the 3D dynamical model we use two collective-shape coordinates $(c,h,\alpha = 0)$ plus the projection of total spin of the compound nucleus on the symmetry axis. Furthermore, in the 4D and 3D dynamical models, we use the chaos weighted wall and window friction formula to reproduce the average kinetic energies of fission fragments, the pre-scission neutron multiplicities, the fission time, and the variances of the mass and kinetic energy of fission fragments for the excited compound nuclei ^{256}Fm, ^{215}Fr, ^{187}Ir ^{172}Yb, ^{162}Yb, and ^{142}Ce.

The main purpose of this research is to investigate how the asymmetry parameter and dissipation coefficient of the K

*eslamizadeh@pgu.ac.ir

coordinate influences different aspects of fission of excited compound nuclei over a wide range of mass number.

The present paper is arranged as follows: In Sec. II, we describe the models and basic equations. The results of the calculations are presented in Sec. III. Finally, the concluding remarks are given in Sec. IV.

II. DESCRIPTION OF MODEL

We use a stochastic approach based on multidimensional Langevin equations to treat the symmetry and asymmetric fission process of some compound nuclei produced in fusion reactions. In our calculations, we use the 3D Langevin dynamical model developed in Refs. [26–28] by adding the orientation degree of freedom (K coordinate) to three collective coordinates $\boldsymbol{q} = (q_1,q_2,q_3) = (c,h,\alpha)$ [29]. The parameter c is the half length of the nucleus, h describes a variation in thickness of the neck for a given elongation of the nucleus, and α is the asymmetry parameter. In the stochastic approach the evolution of the collective coordinates can be treated as the motion of a Brownian particle placed in a viscous heat bath [30,31]. The coupled Langevin equations for describing the dynamics of the collective coordinates have the following form:

$$
\begin{aligned}
q_i^{(n+1)} &= q_i^{(n)} + \frac{1}{2}\mu_{ij}^{(n)}(\boldsymbol{q})\left(p_j^{(n)} + p_j^{(n+1)}\right)\tau, \\
p_i^{(n+1)} &= p_i^{(n)} - \tau\left[\frac{1}{2}p_j^{(n)}p_k^{(n)}\left(\frac{\partial\mu_{jk}(\boldsymbol{q})}{\partial q_i}\right)^{(n)} - Q_i^{(n)}(\boldsymbol{q}) - \gamma_{ij}^{(n)}(\boldsymbol{q})\mu_{ik}^{(n)}(\boldsymbol{q})p_k^{(n)}\right] + \theta_{ij}^{(n)}\xi_j^{(n)}\sqrt{\tau},
\end{aligned}
\tag{1}
$$

where m_{ij} ($\|\mu_{ij}\| = \|m_{ij}\|^{-1}$) is the tensor of inertia, q_i and p_i are the collective coordinates and their conjugate momenta, γ_{ij} is the friction tensor, $\theta_{ij}\xi_j$ is a random force, θ_{ij} is its amplitude, and ξ_j is a random variable that possesses the following statistical properties: $\langle\xi_i\rangle = 0$ and $\langle\xi_i(t_1)\xi_j(t_2)\rangle = 2\delta_{ij}\delta(t_1 - t_2)$. The superscript n in Eq. (1) shows that the corresponding quantity is calculated at the instant $t_n = n\tau$, where τ is the integration time step of the Langevin equations. Q_i is a conservative force and can be given by the Helmholtz free energy

$$
Q_i(\boldsymbol{q},I,K) = -\left(\frac{\partial F}{\partial q_i}\right)_T. \tag{2}
$$

The Helmholtz free energy can be determined in terms of the potential energy and level density parameter as follows:

$$
F(\boldsymbol{q},I,K) = V(\boldsymbol{q},I,K) - a(\boldsymbol{q})T^2. \tag{3}
$$

From Eqs. (2) and (3), it follows that the conservation force in the Fermi gas model has the form

$$
Q_i(\boldsymbol{q},I,K) = -\frac{\partial V(\boldsymbol{q},I,K)}{\partial q_i} + \frac{\partial a(\boldsymbol{q})}{\partial q_i}T^2, \tag{4}
$$

where the deformation dependence of the level-density parameter can be obtained as [32]

$$
a(\boldsymbol{q}) = 0.073A + 0.095A^{2/3}B_S(\boldsymbol{q}). \tag{5}
$$

where A and $B_S(\boldsymbol{q})$ are mass number and surface energy of the compound nucleus, respectively. During a random walk along the Langevin trajectory, conservation of energy is satisfied by

$$
E^* = E_{\rm int}(t) + E_{\rm coll}(\boldsymbol{q},\boldsymbol{p}) + V(\boldsymbol{q},I,K) + E_{\rm evap}(t), \tag{6}
$$

where E^* is the total excitation energy of the compound nucleus, $E_{\rm int}$ is the intrinsic excitation energy of the nucleus, $E_{\rm coll} = 0.5\mu_{ij}(\boldsymbol{q})p_i p_j$ is the kinetic energy of the collective motion of the nucleus, $V(\boldsymbol{q},I,K)$ is the potential energy, $E_{\rm evap}(t)$ is the energy carried away by evaporated particles by time t. In cylindrical coordinates, the surface of the nucleus is given by

$$
\rho_S^2(z) = \begin{cases} (c^2 - z^2)(A_s + Bz^2/c^2 + az/c), & B \geqslant 0 \\ (c^2 - z^2)[A_s + \alpha z/c)\exp(Bcz^2)], & B < 0, \end{cases} \tag{7}
$$

where ρ_S is the polar radius and z is the coordinate along the symmetry axis of the nucleus. The coefficients B and A_s in Eq. (7) can be expressed in terms of the nuclear shape parameters c,h, and α as follows:

$$
B = 2h + \frac{c-1}{2}, \tag{8}
$$

$$
A_s = \begin{cases} c^{-3} - \frac{B}{5}, & B \geqslant 0 \\ -\frac{4}{3}\frac{B}{\exp(Bc^3) + (1+\frac{1}{2Bc^3})\sqrt{-\pi Bc^3}\,\mathrm{erf}(\sqrt{-Bc^3})}, & B < 0, \end{cases} \tag{9}
$$

where $\mathrm{erf}(x)$ is the error function.

The friction tensor is calculated by the chaos weighted wall and window friction formula. For small elongation before neck formation, the chaos weighted wall formula is used to calculate the friction tensor and, after neck formation used the chaos

weighted wall and window friction formula [33] as follows

$$\gamma_{ij} = \begin{cases} \mu(\boldsymbol{q})\gamma_{ij}^{\text{wall}} & \text{for nuclear shapes featuring no neck} \\ \mu(\boldsymbol{q})\gamma_{ij}^{\text{wall}} + \gamma_{ij}^{\text{win}} & \text{for nuclear shapes featuring a neck} \end{cases}. \tag{10}$$

The chaoticity μ is a measure of chaos in the single particle motion and depends on the shape of the nucleus. The magnitude of the chaoticity μ changes from 0 to 1 as the nucleus evolves from spherical to a deformed shape. $\gamma_{ij}^{\text{wall}}$ and γ_{ij}^{win} can be determined as in Refs. [33,34]. For nuclear shapes featuring no neck,

$$\gamma_{ij}^{\text{wall}} = \frac{\pi\rho_m}{2}\bar{v}\int_{z_{\min}}^{z_{\max}}\left(\frac{\partial\rho_S^2}{\partial q_i}\right)\left(\frac{\partial\rho_S^2}{\partial q_j}\right)\left[\rho_S^2+\left(\frac{1}{2}\frac{\partial\rho_S^2}{\partial z}\right)^2\right]^{-1/2}dz, \tag{11}$$

and for nuclear shapes featuring a neck,

$$\begin{aligned}\gamma_{ij}^{\text{wall}} = \frac{\pi\rho_m}{2}\bar{v}\Bigg\{&\int_{z_{\min}}^{z_N}\left(\frac{\partial\rho_S^2}{\partial q_i}+\frac{\partial\rho_S^2}{\partial z}\frac{\partial D_1}{\partial q_i}\right)\left(\frac{\partial\rho_S^2}{\partial q_j}+\frac{\partial\rho_S^2}{\partial z}\frac{\partial D_1}{\partial q_j}\right)\left[\rho_S^2+\left(\frac{1}{2}\frac{\partial\rho_S^2}{\partial z}\right)^2\right]^{-1/2}dz \\ &+\int_{z_N}^{z_{\max}}\left(\frac{\partial\rho_S^2}{\partial q_i}+\frac{\partial\rho_S^2}{\partial z}\frac{\partial D_2}{\partial q_i}\right)\left(\frac{\partial\rho_S^2}{\partial q_j}+\frac{\partial\rho_S^2}{\partial z}\frac{\partial D_2}{\partial q_j}\right)\left[\rho_S^2+\left(\frac{1}{2}\frac{\partial\rho_S^2}{\partial z}\right)^2\right]^{-1/2}dz\Bigg\},\end{aligned} \tag{12}$$

$$\gamma_{ij}^{\text{win}} = \frac{1}{2}\pi\rho_m\bar{v}\left(\frac{\partial R}{\partial q_i}\frac{\partial R}{\partial q_j}\right)\Delta\sigma, \tag{13}$$

where $z_{\min}$ and $z_{\max}$ are the left and right ends of the nuclear shape, z_N is the position of the neck plane that divides the nucleus into two parts, ρ_S is the radial coordinate of the nuclear surface, D_1 and D_2 are the positions of the mass centers of the two parts of the fissioning system relative to the center of mass of the whole system, ρ_m is the mass density of the nucleus, $\bar{v}$ is the average nucleon speed inside the nucleus, R is the distance between the centers of mass of future fragments, and $\Delta\sigma$ is an area of the window between two parts of the system. The inertia tensor is calculated in the Werner–Wheeler approximation for the incompressible and irrotational flow [35]. The rotational part of the potential energy is calculated by

$$\begin{aligned}E_{\text{rot}}(\boldsymbol{q},I,K) &= \frac{\hbar^2K^2}{2J_{||}(\boldsymbol{q})}+\frac{\hbar^2[I(I+1)-K^2]}{2J_{\perp}(\boldsymbol{q})} \\ &= \frac{\hbar^2I(I+1)}{2J_{\perp}(\boldsymbol{q})}+\frac{\hbar^2K^2}{2J_{\text{eff}}(\boldsymbol{q})},\end{aligned} \tag{14}$$

where I is the spin of a compound nucleus and K is the projection of I on the symmetry axis of the nucleus. $J_{||}$ is the rigid body moment of inertia of the nucleus parallel to its symmetry axis, while $J_{\perp}$ is the rigid body moment of inertia perpendicular to the symmetry axis. The rigid body moments of inertia about and perpendicular to the symmetry axis can be determined as in Ref. [36]. J_{eff} is the effective moment of inertia. The inverse of the effective moment of inertia can be determined by $J_{\text{eff}}^{-1} = J_{||}^{-1} - J_{\perp}^{-1}$.

In our calculations, we consider the evolution of the K collective coordinate by using the Langevin equation for overdamped motion as in Ref. [22]:

$$K^{(n+1)} = K^{(n)} - \frac{\gamma_K^2I^2}{2}\frac{\partial E_{\text{rot}}}{\partial K}\tau + \gamma_K I\xi(t)\sqrt{T\tau}, \tag{15}$$

where γ_K is a parameter controlling the coupling between the orientation degree of freedom K and the heat bath, $\xi(t)$ is a random number from a normal distribution with unit variance, and T is the heat bath temperature. The authors of Refs. [22,37] showed that, in the case of a dinucleus, γ_K can be obtained as

$$\gamma_K = \frac{1}{RR_N\sqrt{2\pi^3n_0}}\sqrt{\frac{J_R|J_{\text{eff}}|J_{||}}{J_{\perp}^3}}, \tag{16}$$

where $n_0 = 0.0263\,\text{MeV zs fm}^{-4}$ is the bulk flux in the standard nuclear matter [38], R_N is the neck radius, R is the distance between the centers of mass of the nascent fragments and $J_R = M_0R^2/4$ for a reflection symmetric shape. For the case of mononuclear shapes without a neck, the results of Eq. (16) can be extrapolated as in Ref. [1]. Figure 1 shows the dissipation coefficient of K as a function of the collective coordinate q_1 for the compound nucleus ^{215}Fr. It should be mentioned that the constant parameter γ_K is usually used in dynamical investigations of the K coordinate time evolution. The value $\gamma_K = 0.077\,(\text{MeV zs})^{-1/2}$ was found reasonable. The magnitude of this parameter was estimated by reproducing

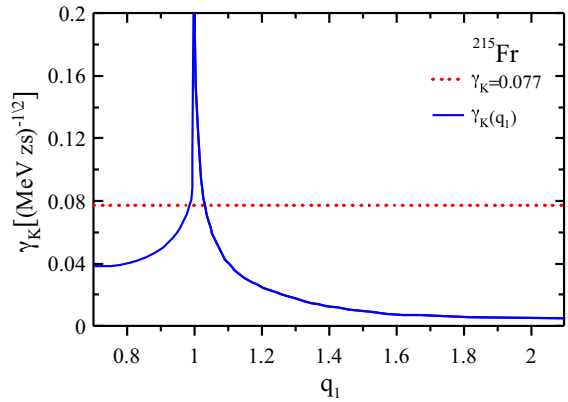

FIG. 1. The dissipation coefficient of K as a function of the collective coordinate q_1 for the compound nucleus ^{215}Fr. The dotted line corresponds to $\gamma_K = 0.077\,(\text{MeV zs})^{-1/2}$.

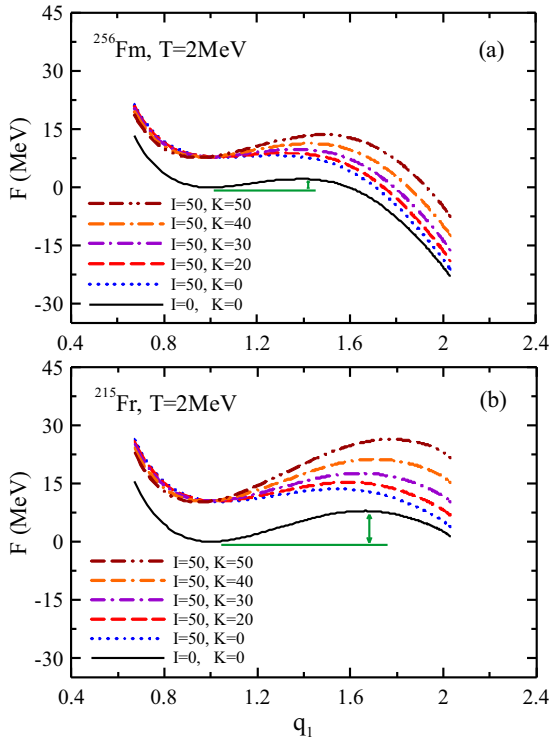

FIG. 2. The Helmholtz free energy for the compound nuclei (a) ^{256}Fm and (b) ^{215}Fr as a function of the collective coordinate q_1 and for different combinations of I and K values at $T = 2$ MeV.

experimental data on angular distributions of fission fragments [39].

The potential energy is calculated on the basis of the liquid drop model with a finite range of nuclear forces [40] using the parameters from Ref. [41],

$$V(\boldsymbol{q},I,K) = [B_S(\boldsymbol{q}) - 1]E_S^0(A,Z) + [B_C(\boldsymbol{q}) - 1]E_C^0(A,Z) + E_{\rm rot}(\boldsymbol{q},I,K), \quad (17)$$

where $B_S(\boldsymbol{q})$ and $B_C(\boldsymbol{q})$ are surface- and Coulomb-energy terms, respectively. $B_S(\boldsymbol{q})$ and $B_C(\boldsymbol{q})$ can be calculated as in Ref. [40]. E_S^0 and E_C^0 are the surface and Coulomb energies of a spherical nucleus, respectively. In Figs. 2 and 3 we compare the Helmholtz free energy calculated for the compound nuclei ^{256}Fm, ^{215}Fr, and ^{187}Ir as a function of the collective coordinate q_1 and for different combinations of I and K values at $T = 2$ MeV. It is clear from Figs. 2 and 3 that, for a given value of spin, the height of the potential-energy surface increases with increasing K. Such an increase of the fission barrier will increase the fission time and consequently increase the number of evaporated pre-scission particles. It can also be seen from Figs. 2 and 3 that the inclusion of the K coordinate not only changes the fission barrier height but also affects the saddle-point configuration. It is clear from Figs. 2 and 3 that the distance between the ground state and saddle point decreases with increasing mass number of nuclei. Furthermore, it can be seen from Fig. 3 that the inclusion of the K coordinate in the calculation of the potential energy shifts the saddle point toward the scission point.

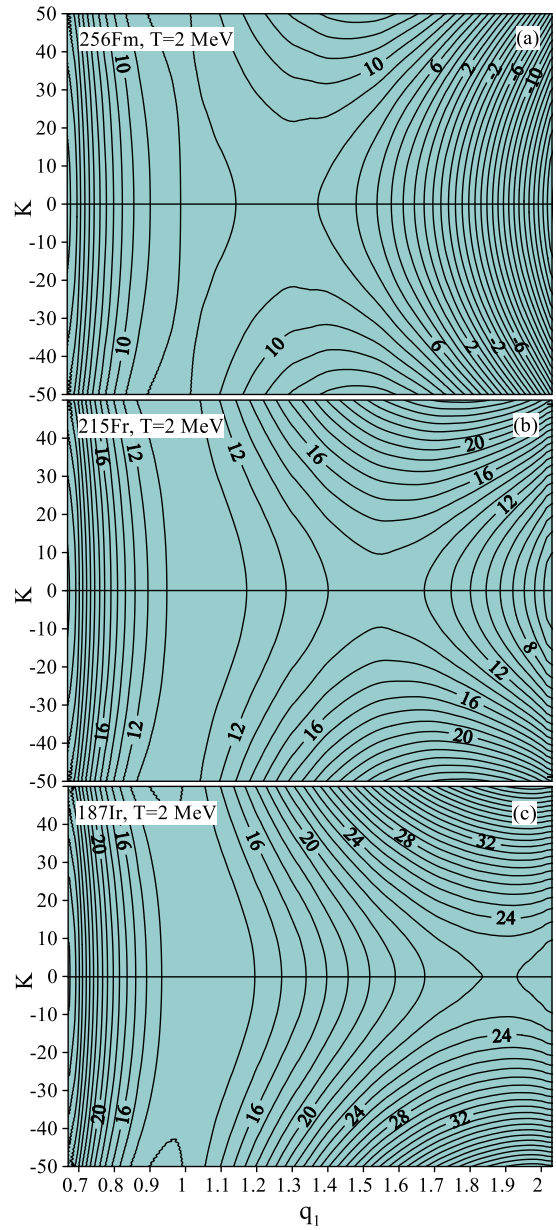

FIG. 3. The Helmholtz free energy for the compound nuclei (a) ^{256}Fm, (b) ^{215}Fr, and (c) ^{187}Ir as a function of the collective coordinates q_1 and K at $T = 2$ MeV and $I = 50\hbar$. The numbers at the contour lines represent the Helmholtz free energy values in MeV.

In our calculations, we start modeling fission dynamics from the ground state with the excitation energy E^* of the compound nucleus. The initial conditions in the ground state can be chosen by the Neumann method with the generating function

$$\Phi(\boldsymbol{q_0},\boldsymbol{p_0},I,t=0) \propto \exp\left[-\frac{V(\boldsymbol{q_0}) + E_{\rm coll}(\boldsymbol{q_0},\boldsymbol{p_0})}{T}\right]\delta(\boldsymbol{q}-\boldsymbol{q_0})F(I), \quad (18)$$

where $F(I)$ is the spin distribution for heavy-ion complete fusion, which is expressed as

$$F(I) = \frac{2\pi}{k^2}\frac{2I+1}{1+\exp\left(\frac{I-I_c}{\delta I}\right)}, \quad (19)$$

where k is the wave number, δI is the diffuseness, and I_c is the critical spin. The parameters δI and I_c can be approximated by the relations [42]

$$\delta I = \begin{cases} (A_P A_T)^{3/2} \times 10^{-5}[1.5 + 0.02(E_{c.m.} - V_C - 10)] & \text{for } E_{c.m.} > V_C + 10 \\ (A_P A_T)^{3/2} \times 10^{-5}[1.5 - 0.04(E_{c.m.} - V_C - 10)] & \text{for } E_{c.m.} < V_C + 10, \end{cases} \quad (20)$$

and

$$I_c = \sqrt{A_P A_T / A_{CN}}\left(A_P^{1/3} + A_T^{1/3}\right)(0.33 + 0.205\sqrt{E_{c.m.} - V_C}), \quad (21)$$

when $0 < E_{c.m.} - V_C < 120$ MeV; and when $E_{c.m.} - V_C > 120$ MeV the term in the final brackets is set equal to 2.5. In Eqs. (20) and (21) A_T, A_P, and A_{CN} represent the mass of the target, projectile and the compound nucleus, respectively. V_C is the Coulomb barrier. The initial spin for each Langevin trajectory is sampled from the above spin distribution function. Figure 4 shows the calculated results of the spin distribution $F(I)$ for the compound nuclei ^{256}Fm, ^{215}Fr, ^{187}Ir, ^{172}Yb, and ^{142}Ce as a function of spin at $E_{lab} = 158.8$ MeV. It can be seen from Fig. 4 that, at a given energy of the projectile, the heavier compound nucleus formed with a larger spin.

It should be mentioned that the initial K value can be generated by using the Monte Carlo method from the uniform distribution in the interval $(-I, I)$. In the present calculations, we neglect the spins of the projectile and target nuclei and assume that the spin of the compound nucleus is approximately equal to the orbital angular momentum. In the simulation of the fission process of the excited nuclei, the evaporation of pre-scission light particles along the Langevin trajectory can be taken into account by using a Monte Carlo simulation technique. The decay widths for emission n, p, α, and γ can be calculated at each Langevin time step τ as in Refs. [43,44]. The decay widths for emission n, p and α particle can be calculated by the following relation [43]:

$$\Gamma_v = (2s_v + 1)\frac{m_v}{\pi^2\hbar^2\rho_{comp}(E_{int})} \times \int_0^{E_{int}-B_v} d\varepsilon_v \rho_{res}(E_{int} - B_v - \varepsilon_v)\varepsilon_v \sigma_{inv}(\varepsilon_v), \quad (22)$$

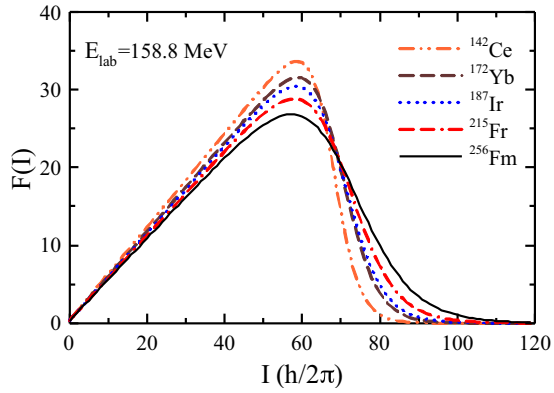

FIG. 4. The spin distribution $F(I)$ for the compound nuclei ^{256}Fm, ^{215}Fr, ^{187}Ir, ^{172}Yb, and ^{142}Ce as a function of spin at $E_{lab} = 158.8$ MeV.

where σ_{inv} is the inverse cross section [43], $\rho_{res}(E_{int} - B_v - \varepsilon_v)$ and $\rho_{comp}(E_{int})$ are the level densities of the residual and compound nuclei, and B_v and ε_v are the separation energy and kinetic energy of the evaporated particle v, respectively. s_v is the spin of the emitted particle v and m_v is its reduced mass with respect to the residual nucleus. The width of the gamma emission is calculated as in Ref. [44]. The loss of spin is taken into account by assuming that each neutron, proton, or γ quanta carries away $1\hbar$ while the α particle carries away $2\hbar$. It should be stressed that the level density is a key physical quantity in the calculations, because it comes in all the disintegration widths. In the calculations of the level density, we take into account the paring corrections, collective vibrations, and rotation in the nuclei as in Ref. [45].

In the simulation of the evolution of a fissile nucleus, a Langevin trajectory either reaches the scission surface and counts as a fission event or, if the excitation energy for a trajectory which is still inside the saddle reaches the value $E_{int} + E_{coll} < \min(B_n, B_f)$, the event is counted as an evaporation residue (B_n is the binding energy of neutron and B_f is the fission-barrier height). In our calculations, we obtain average values of the pre-scission particle multiplicity by using the following relation:

$$\langle M \rangle = \frac{\sum_{I=0}^{I=I_c}\sum_{\alpha=0}^{\alpha=\alpha_f}\langle M\rangle_{I\alpha}(2I+1)P_I}{\sum_{I,\alpha}(2I+1)P_I}, \quad (23)$$

where P_I is the probability of a particle crossing the fission barrier. This can be determined by the ratio of number of the trajectories crossing the barrier for given α, I and the total number of trajectories chosen. I_c and α_f are the critical spin and maximum asymmetry parameter, respectively.

In the calculations, the total kinetic energy E_k of the fission fragments is obtained by the sum of the Coulomb repulsion energy V_C of the fragments, the nuclear attractive energy V_n of the nascent fragments and the kinetic energy of their relative motion E_{ps}:

$$\langle E_k \rangle = \langle V_C \rangle + \langle V_n \rangle + \langle E_{ps} \rangle, \quad (24)$$

and its variance is

$$\sigma_{E_k}^2 = \sigma_{\tilde{V}_C}^2 + \sigma_{E_{ps}}^2 + 2\sigma_{\tilde{V}_C E_{ps}}, \quad (25)$$

where

$$\sigma_{\tilde{V}_C}^2 = \langle \tilde{V}_C^2 \rangle - \langle \tilde{V}_C \rangle^2,$$
$$\sigma_{E_{ps}}^2 = \langle E_{ps}^2 \rangle - \langle E_{ps} \rangle^2, \quad (26)$$
$$\sigma_{\tilde{V}_C E_{ps}} = \langle \tilde{V}_C E_{ps} \rangle - \langle \tilde{V}_C \rangle \langle E_{ps} \rangle,$$

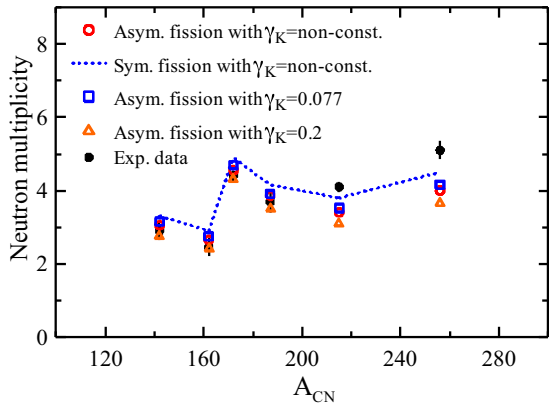

FIG. 5. The pre-scission neutron multiplicity as a function of the compound nuclear mass $A_{\rm CN}$. The open squares, open triangles, and open circles are the calculated results calculated with the 4D Langevin equations and by using $\gamma_K = 0.077\ (\mathrm{MeV\,zs})^{-1/2}$, $\gamma_K = 0.2\ (\mathrm{MeV\,zs})^{-1/2}$ and $\gamma_k =$ nonconstant, respectively. The solid symbols are the experimental data [48].

and

$$\tilde{V}_{\rm C} = V_{\rm C} + V_{\rm n}, \tag{27}$$

The last equation means that a part of the Coulomb repulsion energy is used to overcome the nuclear attraction between the nascent fragments. It can be estimated as in Refs. [46,47].

III. RESULTS AND DISCUSSIONS

In this paper, we apply a stochastic approach based on the 3D and 4D Langevin equations to study the effect of dissipation coefficient of the K coordinate and the asymmetry parameter on different aspects of fission of excited compound nuclei. We calculated the observables in fission of the compound nuclei ^{256}Fm, ^{215}Fr, ^{187}Ir, ^{172}Yb, ^{162}Yb, and ^{142}Ce formed in the following heavy-ion reactions:

(1) $^{18}\mathrm{O} + ^{238}\mathrm{U} \rightarrow ^{256}\mathrm{Fm}\,(E_{\rm lab} = 158.8\,\mathrm{MeV})$;
(2) $^{18}\mathrm{O} + ^{197}\mathrm{Au} \rightarrow ^{215}\mathrm{Fr}\,(E_{\rm lab} = 158.8\,\mathrm{MeV})$;
(3) $^{18}\mathrm{O} + ^{169}\mathrm{Tm} \rightarrow ^{187}\mathrm{Ir}\,(E_{\rm lab} = 158.8\,\mathrm{MeV})$;
(4) $^{18}\mathrm{O} + ^{154}\mathrm{Sm} \rightarrow ^{172}\mathrm{Yb}\,(E_{\rm lab} = 158.8\,\mathrm{MeV})$;
(5) $^{18}\mathrm{O} + ^{144}\mathrm{Sm} \rightarrow ^{162}\mathrm{Yb}\,(E_{\rm lab} = 158.8\,\mathrm{MeV})$;
(6) $^{18}\mathrm{O} + ^{124}\mathrm{Sn} \rightarrow ^{142}\mathrm{Ce}\,(E_{\rm lab} = 158.8\,\mathrm{MeV})$.

In the 4D dynamical model, we used three collective shape coordinates ($q_1 = c$, $q_2 = h$, $q_3 = \alpha$) plus the projection of total spin of the compound nucleus on the symmetry axis, K. In the 3D dynamical model we used two collective shape coordinates ($q_1 = c$, $q_2 = h$, $q_3 = \alpha = 0$) plus the projection of total spin of the compound nucleus on the symmetry axis. In the dynamical calculations for symmetric and asymmetric fission, nuclear dissipation was generated through the chaos weighted wall and window friction formula and the magnitude of the dissipation coefficient of K, γ_k, has been considered as a constant, $\gamma_K = 0.077\ (\mathrm{MeV\,zs})^{-1/2}$, $\gamma_K = 0.2\ (\mathrm{MeV\,zs})^{-1/2}$, and a nonconstant value according to Eq. (16). The pre-scission neutron multiplicities, the fission time, the average kinetic energies of fission fragments, and the variances of the mass and kinetic

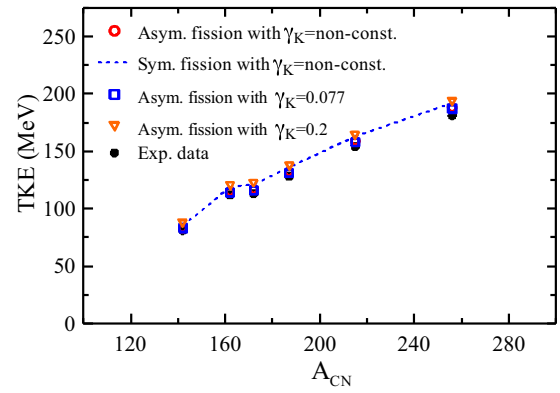

FIG. 6. Same as Fig. 5 but for the average kinetic energies of fission fragments as a function of the compound nuclear mass $A_{\rm CN}$. The solid symbols are the experimental data [48].

energy of fission fragments have been calculated for symmetric and asymmetric fission of the compound nuclei ^{256}Fm, ^{215}Fr, ^{187}Ir, ^{172}Yb, ^{162}Yb, ^{142}Ce and results of the calculations compared with each other and with the experimental data. Figures 5–7 show the results of the pre-scission neutron multiplicities, the average kinetic energies of fission fragments, and the fission time as a function of mass number of the compound nuclei $A_{\rm CN}$ calculated for symmetric and asymmetric fission by using $\gamma_K = 0.077\ (\mathrm{MeV\,zs})^{-1/2}$, $\gamma_K = 0.2\ (\mathrm{MeV\,zs})^{-1/2}$, and $\gamma_K =$ nonconstant.

It can be seen from Fig. 6 that the differences between the calculated data calculated with the 4D and 3D dynamical models and by using $\gamma_K = 0.077\ (\mathrm{MeV\,zs})^{-1/2}$, $\gamma_K = 0.2\ (\mathrm{MeV\,zs})^{-1/2}$ and $\gamma_k =$ nonconstant are small. It can also be seen from Figs. 5 and 7 that, for intermediate nuclei, the differences between the calculated data calculated with the different values of γ_K are small, although the differences between the calculated values themselves and with the experimental data increase with increasing mass number of the excited compound nuclei. It is clear from Figs. 5 and 7 that the calculated data for heavy nuclei are slightly lower than the experimental data. It is also clear from Figs. 5 and 7 that the results of symmetric

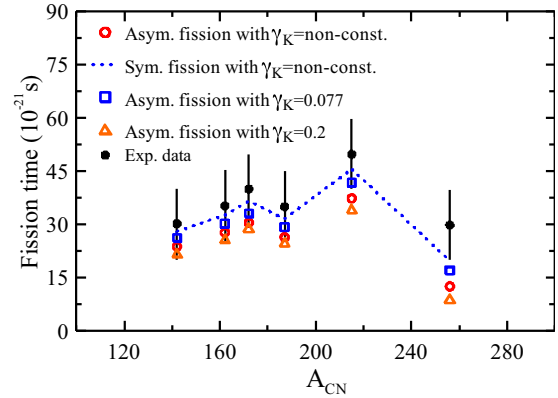

FIG. 7. Same as Fig. 5 but for the fission time as a function of the compound nuclear mass $A_{\rm CN}$. The solid symbols are the experimental data [48].

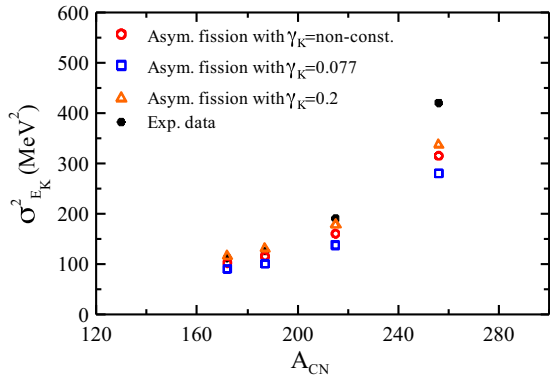

FIG. 8. The results of calculations for variance of the kinetic energy distribution of fission fragments as a function of the compound nuclear mass $A_{\rm CN}$. The open squares, open triangles, and open circles are the calculated results calculated with the 4D Langevin equations and by using $\gamma_K = 0.077\ (\text{MeV zs})^{-1/2}$, $\gamma_K = 0.2\ (\text{MeV zs})^{-1/2}$ and $\gamma_k =$ nonconstant, respectively. The solid circles are the experimental data [48].

simulations by using $\gamma_k =$ nonconstant are in better agreement with the experimental data. According to the results obtained for pre-scission neutron multiplicity and fission time, it can be concluded that, for heavy nuclei, the strength of the nuclear dissipation needs to be increased. Furthermore, it can also be seen from Fig. 5 that the observed multiplicities increase with the increase in the compound nuclear mass in general and show some fluctuations. The fluctuations in the observed and calculated multiplicity may be due to specific structure effects.

We have also calculated the variance of the kinetic-energy distribution and the variance of mass distribution of fission fragments for the above-mentioned fusion-fission reactions. The results of calculations for asymmetric fission and by using different values of the dissipation coefficient of K are presented in Figs. 8 and 9.

It can be seen from Figs. 8 and 9 that the differences between the calculated data with the experimental data for intermediate nuclei calculated with the 4D dynamical model and by

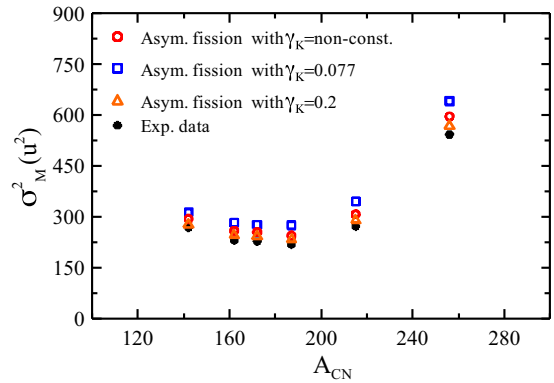

FIG. 9. Same as Fig. 8 but for the variance of mass distribution of fission fragments as a function of the compound nuclear mass $A_{\rm CN}$. The solid symbols are the experimental data [48].

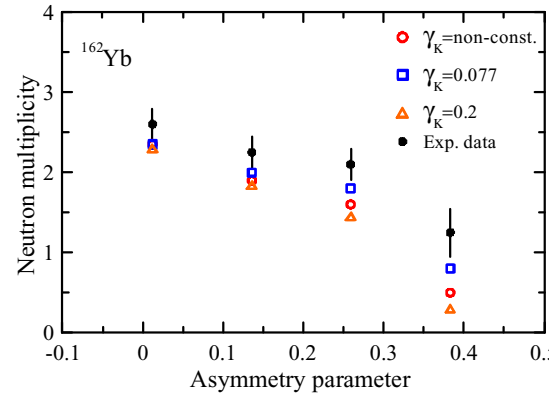

FIG. 10. The pre-scission neutron multiplicity as a function of the asymmetry parameter for the compound nucleus ^{162}Yb calculated with the 4D dynamical model and by using different values of γ_K. The solid circles are the experimental data [48].

using $\gamma_k =$ nonconstant, $\gamma_K = 0.077\ (\text{MeV zs})^{-1/2}$ and $\gamma_K = 0.2\ (\text{MeV zs})^{-1/2}$ are small, although the differences between the calculated data with each other and with the experimental data increase with increasing mass number of the excited compound nucleus. It is also clear from Figs. 8 and 9 that the calculated results calculated with the 4D dynamical model and by using $\gamma_K = 0.2\ (\text{MeV zs})^{-1/2}$ are more in agreement with the experimental data. In the present investigation, we have also calculated the pre-scission neutron multiplicity as a function of the asymmetry parameter for the compound nucleus ^{162}Yb. Figure 10 shows the predicted pre-scission neutron multiplicity as a function of the asymmetry parameter for the compound nucleus ^{162}Yb.

It is evident from the Fig. 10 that the predicted values of pre-scission neutron multiplicity calculated with the 4D Langevin equations are strongly dependent on the fragment asymmetry. It is also clear from Fig. 10 that the calculated values for pre-scission neutron multiplicity decrease rapidly with the increase in fragment asymmetry.

IV. CONCLUSIONS

The average kinetic energies of fission fragments, the pre-scission neutron multiplicities, the fission time and the variances of the mass and kinetic energy of fission fragments have been calculated in a wide range of mass number for the excited compound nuclei ^{256}Fm, ^{215}Fr, ^{187}Ir, ^{172}Yb, ^{162}Yb, and ^{142}Ce by solving 3D and 4D Langevin equations with dissipation generated through the chaos weighted wall and window friction formula. The constant dissipation coefficients of K equal to $\gamma_K = 0.077\ (\text{MeV zs})^{-1/2}$, $\gamma_K = 0.2\ (\text{MeV zs})^{-1/2}$ and a nonconstant dissipation coefficient of K have been used to reproduce the experimental data for both symmetric and asymmetric fission, and the results of the calculations compared with each other and with the experimental data. Comparison of the theoretical results with the experimental data shows that the differences between the results of calculations calculated by using different values of γ_K for symmetric and asymmetric simulations of the fission process of the excited intermediate compound nuclei are

low, whereas for heavy compound nuclei are slightly high. In other words, the effect of asymmetry parameter on the fission process of intermediate nuclei is smaller than heavy nuclei. Furthermore, it is shown that the pre-scission neutron multiplicity decreases rapidly with the increase in fragment asymmetry.

ACKNOWLEDGMENTS

The authors thank the anonymous referee for comments and suggestions, which led to a significantly improved version of this paper. Support from the Research Committee of the Persian Gulf University is greatly acknowledged.

[1] P. N. Nadtochy, E. G. Ryabov, and G. D. Adeev, J. Phys. G: Nucl. Part. Phys. **42**, 045107 (2015).
[2] P. N. Nadtochy, E. G. Ryabov, A. V. Cheredov, and G. D. Adeev, Eur. Phys. J. A **52**, 308 (2016).
[3] K. Mazurek, P. N. Nadtochy, E. G. Ryabov, and G. D. Adeev, Eur. Phys. J. A **53**, 79 (2017).
[4] K. -H Schmidt, and B. Jurado, Eur. Phys. J. A **51**, 176 (2015).
[5] H. Eslamizadeh, Phys. Rev. C **94**, 044610 (2016).
[6] H. Eslamizadeh, J. Phys. G: Nucl. Part. Phys. **42**, 095103 (2015).
[7] A. V. Karpov, P. N. Nadtochy, E. G. Ryabov, and G. D. Adeev, J. Phys. G: Nucl. Part. Phys. **29**, 2365 (2003).
[8] H. Eslamizadeh, Eur. Phys. J. A **50**, 186 (2014).
[9] V. Y. Denisov, T. O. Margitych, and I. Y. Sedykh, Nucl. Phys. A **958**, 101 (2017).
[10] G. G. Adamian, N. V. Antonenko, L. A. Malov, G. Scamps, and D. Lacroix, Phys. Rev. C **90**, 034322 (2014).
[11] H. Eslamizadeh, Int. J. Mod. Phys. E **21**, 1250008 (2012).
[12] J. Tian, N. Wang, and W. Ye, Phys. Rev. C **95**, 041601 (2017).
[13] W. Ye and J. Tian, Phys. Rev. C **93**, 044603 (2016).
[14] H. Eslamizadeh, Int. J. Mod. Phys. E **24**, 1550052 (2015).
[15] H. Eslamizadeh and M. Soltani, Ann. Nucl. Energy **80**, 261 (2015).
[16] I. I. Gontchar, D. J. Hinde, M. Dasgupta, and J. O. Newton, Phys. Rev. C **69**, 024610 (2004).
[17] M. V. Chushnyakova and I. I. Gontchar, Phys. Rev. C **87**, 014614 (2013).
[18] H. Eslamizadeh, J. Phys. G: Nucl. Part. Phys. **44**, 025102 (2017).
[19] J. Randrup, P. Möller, and A. J. Sierk, Phys. Rev. C **84**, 034613 (2011).
[20] H. Eslamizadeh and E. Ahadi, Phys. Rev. C **96**, 034621 (2017).
[21] J. P. Lestone, Phys. Rev. C **59**, 1540 (1999).
[22] J. P. Lestone and S. G. McCalla, Phys. Rev. C **79**, 044611 (2009).
[23] P. N. Nadtochy, E. G. Ryabov, A. E. Gegechkori, Yu. A. Anischenko, and G. D. Adeev, Phys. Rev. C **89**, 014616 (2014).
[24] P. N. Nadtochy, E. G. Ryabov, A. E. Gegechkori, Yu. A. Anischenko, and G. D. Adeev, Phys. Rev. C **85**, 064619 (2012).
[25] Yu. A. Anischenko, A. E. Gegechkori, and G. D. Adeev, Acta Phys. Pol. B **42**, 493 (2011).
[26] P. N. Nadtochy, G. D. Adeev, and A. V. Karpov, Phys. Rev. C **65**, 064615 (2002).
[27] A. V. Karpov, P. N. Nadtochy, D. V. Vanin, and G. D. Adeev, Phys. Rev. C **63**, 054610 (2001).
[28] A. V. Karpov, R. M. Hiryanov, A. V. Sagdeev, and G. D. Adeev, J. Phys. G: Nucl. Part. Phys. **34**, 255 (2007).
[29] M. Brack, J. Damgaard, A. S. Jensen, H. C. Puli, and V. M. Strutinsky, Rev. Mod. Phys. **44**, 320 (1972).
[30] H. A. Kramers, Physica (Amesterdam) **7**, 284 (1940).
[31] Y. Abe, C. Grégoire, and H. Delagrange, J. Phys. C **47**, C4–329 (1986).
[32] A. V. Ignatyuk, M. G. Itkis, V. N. Okolovich, G. N. Smirenkin, and A. S. Tishin, Yad. Fiz. **21**, 1185 (1975).
[33] S. Pal and T. Mukhopadhyay, Phys. Rev. C **57**, 210 (1998).
[34] D. V. Vanin, G. I. Kosenko, and G. D. Adeev, Phys. Rev. C **59**, 2114 (1999).
[35] K. T. R. Davies, A. J. Sierk, and J. R. Nix, Phys. Rev. C **13**, 2385 (1976).
[36] K. T. R. Davies and J. R. Nix, Phys. Rev. C **14**, 1977 (1976).
[37] S. G. McCalla and J. P. Lestone, Phys. Rev. Lett. **101**, 032702 (2008).
[38] T. Døssing and J. Randrup, Nucl. Phys. A **433**, 215 (1985).
[39] J. P. Lestone, A. A. Sonzogni, M. P. Kelly, and R. Vandenbosch, J. Phys. G: Nucl. Part. Phys. **23**, 1349 (1997).
[40] H. J. Krappe, J. R. Nix and A. J. Sierk, Phys. Rev. C **20**, 992 (1979).
[41] A. J. Sierk, Phys. Rev. C **33**, 2039 (1986).
[42] P. Fröbrich and I. I. Gontchar, Phys. Rep. **292**, 131 (1998).
[43] M. Blann, Phys. Rev. C **21**, 1770 (1980).
[44] J. E. Lynn, *The Theory of Neutron Resonance Reactions* (Clarendon, Oxford, 1968), p. 325.
[45] A. V. Ignatyuk, K. K Istekov, and G. N. Smirekin, Sov. J. Nucl. Phys. **29**, 875 (1979).
[46] J. Bao *et al.*, Z. Phys. A **352**, 321 (1995).
[47] S. K. Samaddar, D. Sperber, M. Zielinska-Pfabé, and M. I. Sobel, Phys. Scr. **25**, 517 (1982).
[48] D. J. Hinde, D. Hilscher, H. Rossner, B. Gebauer, M. Lehmann, and M. Wilpert, Phys. Rev. C **45**, 1229 (1992).